Brittle – Ductile Transition and Scatter in Fracture Toughness of Ferritic Steels

S. J. Noronha[*]

Mechanical & Aerospace Engineering Department, University of California, Los Angeles
420 Westwood Plaza, Los Angeles, California, USA
E-mail: snoronha@ucla.edu

N. M. Ghoniem

Mechanical & Aerospace Engineering Department, University of California, Los Angeles
420 Westwood Plaza, Los Angeles, California, USA
E-mail: ghoniem@ucla.edu

Here we analyze a dislocation simulation model for the brittle-to-ductile transition of Ferritic Steels, a typical multiphase material. The crack tip plastic zones are simulated as arrays of discrete dislocations emitted from crack-tip sources and equilibrated against the friction stress due to lattice and obstacles. The crack-tip gets blunted and the emitted dislocation arrays modify the elastic field of the crack. The combined stress field of the crack and the emitted dislocations describe an elasto-plastic crack field. The simulated crack system involves microcracks embedded in the plastic zone of a macrocrack. The inherent scatter in fracture toughness measurements are studied by using a size distribution for microcracks, distributed on the plane of the macrocrack. The scatter in fracture toughness measurements is found to be an effect of the size distribution of microcracks rather than their spatial distribution on the matrix ahead of the crack plane.

[*] Speaker

1. Introduction

Predicting the brittle-ductile transition in multiphase materials like steels pose a scientific and technological challenge. Factors that influence the transition include change in fundamental material properties of the Fe matrix with temperature as well as the microstructural properties like grain sizes, carbide size distribution, etc. Typical microstructure of these materials have brittle precipitates (like carbides and sulphides) embeded in BCC Fe matrix. Now it is a well known fact that fracture in these materials at low temperature is originated in microcracks; and propragtion of these microcracks to the matrix is the critical step that lead to fracture [1].

Discrete dislocation simulations of crack-tip plasticity were successful in predicting the brittle-ductile transition (BDT) of simple single crystalline materials e.g.[2],[3]. The advantage of this approach over continuum methods is that the fundamental material properties such as dislocation velocity and their interactions can be treated dynamically. It has been found that the dislocation mobility plays a significant role in determining the transition temperature [3]. However, the variation of dislocation mobility alone cannot explain the BDT behavior of microstructurally complex materials like steels [4]. Recently we introduced a discrete dislocation simulation model in which the effects of blunting are incorporated by using elastic stress fields of blunted cracks which captures the increase in fracture toughness around the transition temperature [5]. Here we analyse the model to study the observed scatter in the measured fracture toughness values around the ductile-brtittle transition temperature (DBTT).

From numerous careful experimental studies conducted on the BDT behavior of steels it is now established that: (a) the measured microscopic fracture stress (at microcracks) is found to be several orders of magnitude higher than that of pure Griffith value [7],[8]; (b) several cracked brittle particles are found to be present in the broken samples [7],[9]; (c) pre-cracks (macrocracks) blunt substantially before the fracture of the specimen occurs at the transition region [10]; and (d) the size of carbides present in the matrix has a Poisson type distribution [11]. These observations were considered and accounted for in the simulations presented here.

2. Model & Method of Calculation

Based on the above experimental observations, the present model has the following features:
   (1) The emission of dislocations and subsequent shielding at the microcrack tip,
   (2) A distribution of mircocracks on the crack plane of a macrocrack, ahead of it.

(3) Cleavage propagation from any one of these microcracks near the main crack leads to failure,

(4) Blunting of macrocrack is accounted for by modifying the elastic crack-tip field of sharp crack, and

(5) The size distribution of microcracks is assumed to follow Posisson distribution.

As shown schematically in Figure 1a, the macrocrack is assumed to be semi-infinite, with dislocation sources close to the crack-tip. Dislocations are emitted simultaneously along the two slip planes, symmetrically oriented to the crack plane and inclined at 70.5° to the crack plane. The initial source position (x_0) along the slip plane is chosen to be *4b*, where *b* is the magnitude of Burgers vector. As the load is increased dislocations are emitted and the crack-tip gets blunted, which is schematically illustrated in figure 1b. The radius of the blunted crack ρ is taken to be equal to $N\,b\,sin\alpha$, where N is the number of dislocations and α is the slip plane angle. As blunting
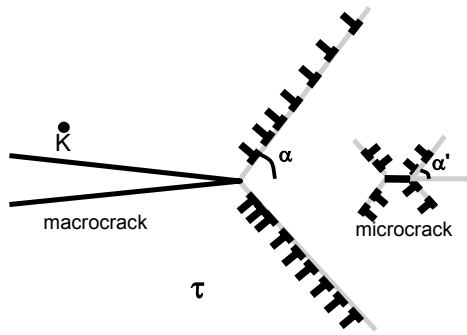

Fig. 1a: The Geometry of the crack and dislocations used in the macrocrack - microcrack simulation model. K is the applied load at the macrocrack, the slip planes angles are oriented at α and α' to the crack planes of macrocrack and microcrack respectively.
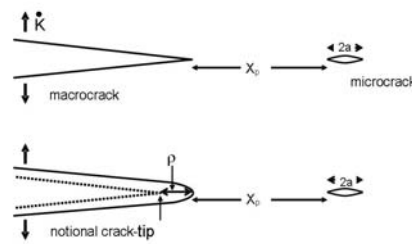
Fig.1b: Schematic illustration of the crack-tip blunting. ρ is the radius of the blunted crack-tip, *2r* the microcrack size and X_p, the distance of the microcrack from macrocrack tip. The distance of the microcrack from the notional sharp crack-tip increases from X_p to $X_p + \rho$.

increases: (a) the crack tip fields are modified to be that of a blunted crack [12], (b) source position is chosen to be equal to the crack-tip radius, i.e. $x_0 = \rho$ (c) the notional crack-tip from which the image stress of dislocations is calculated is moved back to the center of curvature of the blunted crack. The arrays of emitted dislocations form the plastic zones of the crack and the crack may also get blunted due to dislocation emission. The plastic zone developed at the macrocrack modifies the field ahead of it to that of an elastic-plastic material with hardening [13]. During loading, dislocations are emitted from source positions when the resolved shear stress reaches a value $2\tau_y$, where

τ_y is the friction stress experienced by dislocations and is due to the effect of all type

3

of obstacles in dislocation motion including impurities, precipitates, grain boundaries, etc in addition to the lattice friction. The resolved shear stresses are obtained using expressions based on derivations for a finite crack [14] and a semi-infinite crack [15] for respective cases. The emitted dislocations move with a velocity based on the following

expression: $v_{x_i} = \left(\dfrac{\tau_{x_i} - \tau_y}{\tau_{x_i}}\right)\left(|\tau_{x_i}|\right)^m A\, e^{(-Ea/kT)}$ when $|\tau_{x_i}| > \tau_y$, and for $|\tau_{x_i}| < \tau_y$, $v_{x_i} = 0$.

The values for the parameters were obtained by fitting the data of screw dislocation velocities in iron [16]. The value of *m* has a linear dependence on temperature, T, $m = 400/T + 1.2$, $A = 3.14 \times 10^{-4}$ *meters s^{-1} (MPa)$^{-m}$* and E_a =*0.316 eV*. Since the dislocations move only when $|\tau_{x_i}| > \tau_y$ they are in their equilibrium positions at any given time, therefore the temperature and strain rate dependence of measured fracture toughness (K_F), plastic zone size (d_F), crack-tip opening displacement, etc. are determined only by the temperature and strain-rate dependence of the friction stress (τ_y). The applied load is incremented at a rate *dK/dt (=0.01MPa√m s^{-1})*; a variable time step is used to make sure dislocations move as an array and numerical instabilities are avoided. The distribution of microcrack obtained in the previous section is placed ahead of the macrocrack in the crack plane beyond a distance X_{min}=10μm, (which is about a grain diameter). At each time step, the stress ahead of the crack at distances *Xp*'s (the microcracks are assumed to be at these positions) along the crack plane are calculated. The fracture criterion is the tensile stress ($\sigma_{yy}{}^p$) at any of the particle (at distance Xp^i) reaching $\sigma_F{}^i$ (calculated in the previous stage). The applied load at the macrocrack gives the fracture toughness (K_F).

3. Results and Discussion

(a) Microcrack simulation: calculation of microscopic fracture stresses (σ_F)
A microcrack of configuration shown in the inset of Figure 2 is loaded monotonically, dislocation sources emitting dislocations along four symmetric slip planes (α' = 70°5′) around the through thickness crack is used. To mimic the triaxial stress field surrounding the microcrack embedded in the plastic zone of a macrocrack, we modified the expressions for the stress fields given in [14] by subtracting the applied normal stress (σ_{Ay}) and adding the uniaxial yield stress (σ_y) for cases when $\sigma_{Ay} > \sigma_y$. The dislocations are emitted from source positions. Following an earlier study on the effect of source position [11] here we have chosen the source positions as *4b, (b = 2.54Å)*
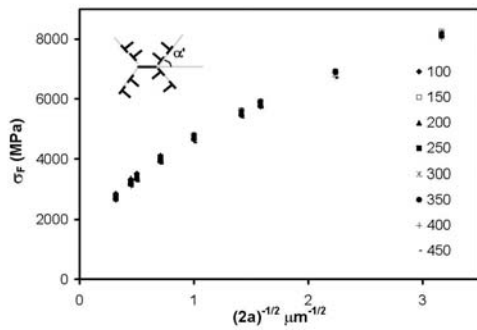
Figure 2a: The microscopic fracture stresses (σ_F) as a function of crack size (*a*), the values of σ_F is shown for different friction stresses (their values in MPa are shown as labels)
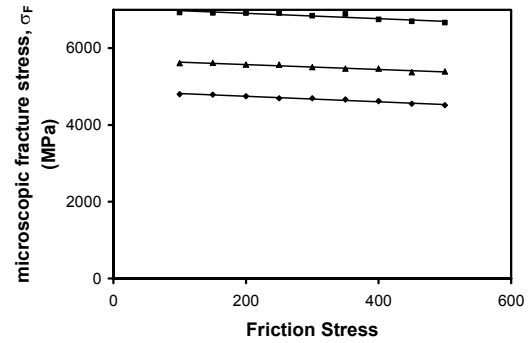
Fig. 2b: The microscopic fracture stress (σ_F) as a function of friction stress for cases with three different microcrack configurations is plotted.

along the slip planes. The stress fields of the emitted dislocations shield the crack-tip from external load. Once moved to their equilibrium position, the amount of shielding from each dislocation is calculated using expressions from [14] and the total shielding at the crack-tip is obtained by summation. The crack-tip stress intensity is calculated at each time step and when it reaches a pre-assigned critical value $k = K_{Ic} = 1.0 MPa\sqrt{m}$ (value estimated for *Fe* with surface energy of *2 Jm^{-2}*), the crack is assumed to propagate and the corresponding applied load is the microscopic fracture stress *(σ_F)*.

The microscopic fracture stress *(σ_F)* is estimated for a range of crack sizes from 0.1 to 5µm. Figure 2a shows the σ_F's as a function of the inverse square root of crack size (*a*), it should be noted that the relation is linear for small crack sizes but deviates for large cracks. The σ_F estimated for different friction stresses is shown in Figure 2b; it should be noted that the fracture stress (σ_F) values of any given crack size is practically independent of temperature consistent with many of the experiments (e.g. [7]). From the best fit curve we interpolate the value of σ_F for a given crack size and friction stress. The value of σ_F's thus obtained is used to calculate the macroscopic fracture toughness (K_F).

(b) Macrocrack simulation: Calculation of Fracture Toughness (K_F)

Figure 3a shows a typical behavior of the tensile stress at the microcrack (σ_{yy}^{p}) position X_P as a function of the applied load (*K*). The fracture criterion in the simulation is σ_{yy}^{p} reaching the critical value σ_F (calculated in the previous stage) at X_P. For the case shown here the size of the microcrack is 1µm, the rate of loading, *dK/dt = 0.01 MPa $\sqrt{m}$s^{-1}*. As the temperature is increased and yield stress (friction stress) is decreased, the applied stress intensity *K* required for the tensile stress at X_P to reach the critical value σ_F increases 'exponentially'. Two factors contributing to this rapid
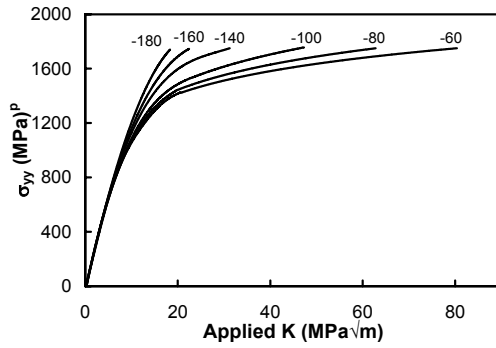
Fig. 3a: The tensile stress at the microcrack (σ_{yy}^{p}) as a function of the (K_{app}) or the simulation time for different yield stresses.
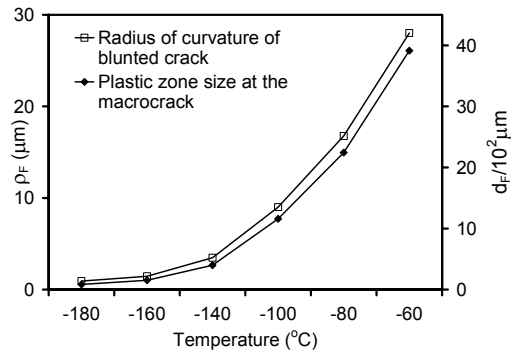
Figure 3b: The crack-tip radius (ρ_F) and the plastic zone size (d_F) calculated at K_F for each temperature is shown.

increase could be the decrease in the tensile stress at the due to the crack-tip blunting and the increasing effects of stress field (predominantly compressive) from the emitted dislocations. This can be seen in Figure *3b* where the plastic zone size (d_F) and the radius of the blunted crack-tip (ρ_F) for each temperature measured at fracture, *K-applied* $= K_F$ is shown. The plastic zone size is the distance measured along the slip plane of the
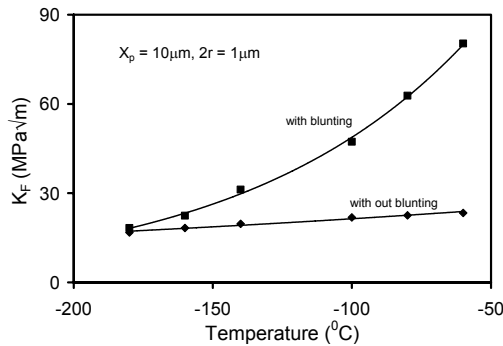

Fig. 4a: The fracture toughness (K_F) as a function of temperature for cases with and without blunting: microcrack size=1μm.
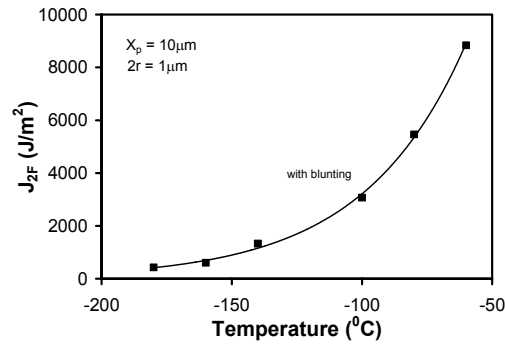
Figure 4b: The J_{2F} – integral calculated for the different temperatures for the blunting case shown in the Figure 5a.

farthest dislocation from the crack-tip. The dislocation source distance (x_0) is chosen as ρ for crack-tip radius greater than *4b*; else $x_0 = 4b$. Figure 4a shows the macroscopic fracture toughness, K_F, as a function of temperature for cases with and without considering the effects of crack-tip blunting. For the case without blunting the increase in the fracture toughness (K_F) with temperature is small. On the other hand, a sharper increase in the fracture toughness is observed when blunting is accounted for in the simulation. This striking observation emphasizes the significant effect of blunting in the

increase of fracture toughness with temperature. This exponential increase in the fracture toughness corresponds to the transition from brittle to ductile behavior.

In Figure 4b the J_{2F}, the J_2 – integral value at fracture, calculated from the number of dislocations emitted at the corresponding load K_F is shown. J_2 is defined as the sum of the glide forces on all dislocations around the crack-tip[17]. In this case, the dislocations are in equilibrium against the friction stress (τ_y) and we can compute J_{2F} as the product of the total number of dislocations (N) and the friction stress (τ_y). Considering the fact that J_{2F} is calculated from the number of dislocations emitted at applied stress intensity factor, K_F, it is striking to note that the pre-factor of the exponent of the J_{2F}- temperature curve (0.0255) matches with that of the K_F-temperature curve (0.0123) in order for the known proportionality between K^2 and J to hold.

(c) Generation of Microcrack Distribution

To mimic the Poisson type distribution [11] of microcracks size in the crack plane (mainly originates from the carbides) we generated microcracks with a Poisson distribution of mean radius of 0.5 µm; and uniformly distributed in a 50µm by 50 µm square region. (The 50 x 50 (µm)^2 region should correspond to the center of an experimental specimen satisfying the plane strain condition). The density of microcracks is taken to be 0.06/µm^2, comparable with the microstructures of typical steels. A typical size distribution of the microcracks used is shown in Figure 5b; in the inset the corresponding distribution is shown. The σ_F's corresponding to each of these microcracks are then estimated from the interpolation of microscopic fracture stress data shown in Figure 2a, and used as input in the next stage of simulation.
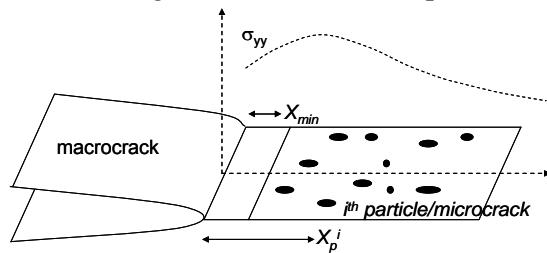

Figure 5a: The Geometry of the model used: A macrocrack with microcracks distributed ahead of it in its crack plane. The propagation of any of the microcracks is the failure criterion in the simulation.
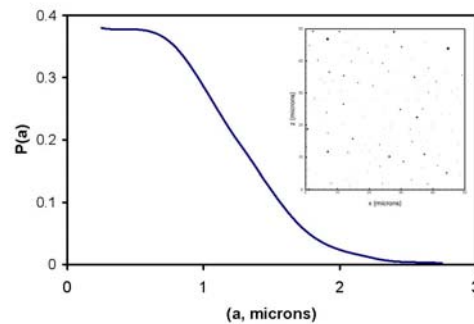
Fig. 5b: The distribution of sizes of the microcracks is shown; a Poisson distribution with mean radius of 0.5µm is used. In the inset a plot of distribution of microcracks uniformly distributed in the crack-plane is shown.

(d) Statistical Analysis of Fracture Toughness (K_F).

We used six different distributions of microcracks for each friction stress values; here we report the results obtained for friction stress values from 200 to 600 MPa. As shown in Figure 4a, when the friction stress is decreased, the applied stress intensity K required for the tensile stress at X_P^i's to reach the critical value σ_F^i increases rapidly.
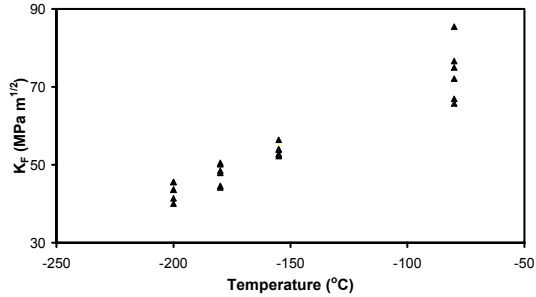

Fig. 6a: The fracture toughness (K_F) as a function of friction stress for cases with six different microcrack configurations is plotted. The mean value curve is also shown.
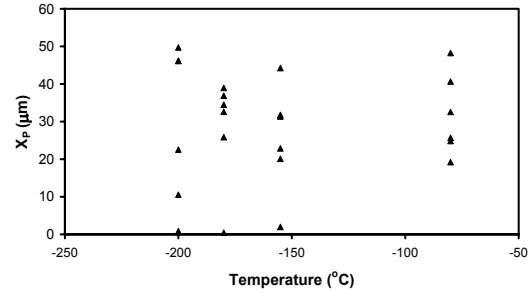
Fig. 6b: The distance of microcracks that leads to fracture in each simulation reported in Figure 4a
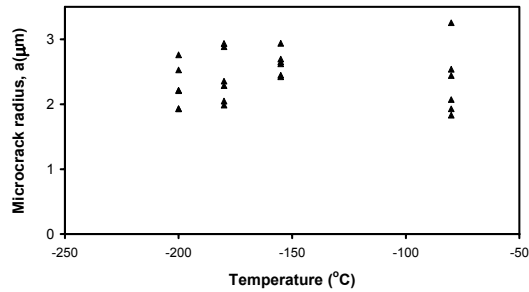

Fig. 6c: The size of microcracks that lead to fracture for different temperatures corresponding to figure 4a.
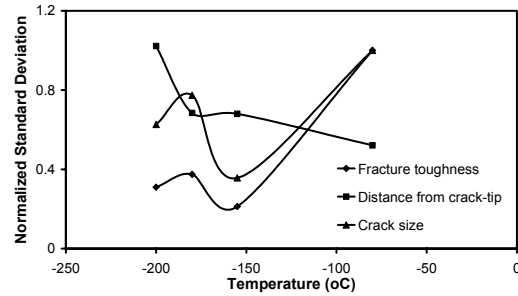
Fig. 6d: The standard deviation of K_F, a, and X_P values respectively plotted in figures 5a, 5b and 5c.

Two factors contributing to this exponential increase could be the decrease in the tensile stress at the microcrack due to the crack-tip blunting and the increasing effects of stress field (predominantly compressive) from the emitted dislocations. This can be seen in Figure *3b,* where the number of dislocations emitted (N_F) and plastic zone size (d_F) for each friction stress measured at fracture, *K-applied* = K_F is shown. The plastic zone size is the distance measured along the slip plane of the farthest dislocation from the crack-tip. This exponential increase in the fracture toughness corresponds to the transition from brittle to ductile behavior.

Figure 6a shows the scatter of the radius of microcracks that leads the fracture. It should be noted that the size of the microcracks that lead to fracture in all the cases are around 2-3μm and the scatter of these values are very narrow; and are independent of the friction stress. On comparing the size of these microcracks with Figure 5b (where a typical size distribution of the crack size is shown), it can be seen that the microcracks

that lead to fracture are among the largest in any given sample. However it should be noted from Figure 5b, that the distance of these microcracks from the macrocrack-tip varies substantially from case to case and is widely scattered. Even though the *Xp* is widely scattered it is found that it is not correlated with the scatter of measured K_F (compare Figures 6a & 6b); whereas it looks like the crack size distribution is correlated to the K_F (compare Figures 6a & 6c) even though their scatter is narrow. Figure 6c shows the normalized (for clarity of display) standard deviation of the values shown in figures 6a, 6b and 6c respectively of K_F, *Xp* and microcrack size (*a*). It can be clearly seen that the standard deviation of K_F is correlated to microcrack size (*a*) and are uncorrelated to X_p.

4. Summary and Conclusions

We presented a dislocation simulation model to study the brittle-ductile transition in Ferritic steels. We found two factors that contribute to the sharp increase in the fracture toughness with temperature: (a) the increase in the mobility of the emitted dislocations, and (b) the effect of crack-tip blunting of the marcocrack. However, usually the experimental measurements of fracture toughness with temperature show wide scatter in values. To address this problem of inherent scatter, we carried out a series of Monte Carlo simulation using a distribution of microcracks situated in the crack plane ahead of the macrocrack. On analysing the statistics of these simulations we found that (a) one among the largest microcracks initiates the fracture in each realization, and (b) the inherent scatter arises from the variation in the size of the microcrack that initiates the fracture and *not* from the variation of its distance from the macrocrack tip.

References

[1] C. J. McMahon Jr, M. Cohen, Acta Metall, 13 (1965) 591.
[2] P. B. Hirsch, S. G. Roberts and J. Samuels, Proc. R Soc. Lond. A, 421 (1989) 25.
[3] P. B. Hirsch and S. G. Roberts, Phil. Mag. A, 64 (1991) 55.
[4] P. B. Hirsch and S. G. Roberts, Phil. Trans. R. Soc. Lond. A 355 (1997) 355.
[5] S. J. Noronha, N. M. Ghoniem, Metall. Mater. Trans. A, 37 (2005) 539.
[6] D. A. Curry and J. F. Knott, Met. Sci., 13 (1979) 341.
[7] P. Bowen, S. G. Druce and J. F. Knott, Acta Metall. 35 (1987) 1735.
[8] S. R. Ortner, C. A. Hippsley, Mater Sci. Tech 12 (1996) 1035.
[9] M. K. Veistinen and V. K. Lindroos, Scripta Metall. 18, (1984) 185.

[10] P. Bowen and J. F. Knott, Metall. Trans. A, 17 (1986) 231.

[11] K. Wallin, T. Saario and K. Törrönen, Metal Sci. 18 (1984) 13.

[12] M. Creager and P. C. Paris, Int. J. Frac. Mech. 3 (1967) 247.

[13] S. G. Roberts, S. J. Noronha, A. J. Wilkinson and P. B. Hirsch, Acta Mater. 50 (2002) 1229.

[14] S. Wang and S. Lee, Mat. Sci. Engin. A130 (1990) 1.

[15] V. Lakshmanan and J. C. M. Li, Mat. Sci. Engin. A104 (1988) 95.

[16] H. Saka, K. Nada and T. Imura, Crystal Lattice Defects 4, (1973) 45.

[17] M. X. Shi, Y. Huang, H. Gao, Int. J. Plasticity, 20 (2004) 1739.